Thermal conductivity by non-equilibrium molecular dynamics using non-locality

Philip B. Allen[1, a)] and Yerong Li[1, 2, b)]

[1)]*Department of Physics and Astronomy, Stony Brook University, Stony Brook, New York 11794-3800, USA*

[2)]*Department of Intensive Instruction, Nanjing University, Nanjing 210093, China*

Non-equilibrium (NE) molecular dynamics (MD), or NEMD, gives a "direct" simulation of thermal conductivity κ. Heat $H(x)$ is added and subtracted in equal amounts ($\int dx H(x) = 0$) at different places x. After steady state is achieved, the temperature $T(x)$ is found by averaging over finite sections. Usually the aim is to extract a value of dT/dx from a place distant from sources and sinks of heat. This yields a value $\kappa_{\text{eff}}(L)$ for the thermal conductivity, L being the system size. The result is then studied as a function of L, to extract the bulk limit κ. Here instead, our heat is $H(x) = H_0 \sin(qx)$, where $q = 2\pi/L$. This causes a steady-state temperature $T_0 + \Delta T \sin(2\pi x/L)$. A thermal conductivity $\tilde{\kappa}(q)$ is extracted, which is well converged at the chosen q. Bulk conductivity κ requires taking the $q \to 0$ limit. The method is tested for liquid and crystalline argon. There are nice advantages in reduced computational noise at a given total MD run time. Another advantage is that $\tilde{\kappa}(q)$ has a more physical meaning than $\kappa_{\text{eff}}(L)$. It can be easily studied using Peierls-Boltzmann transport theory. New results for $\tilde{\kappa}(q)$ in simplified Debye-type models give new insight about extrapolation to $q \to 0$ or $1/L \to 0$. In particular, it is shown that $\kappa_{\text{eff}}(L)$ is unlikely to behave as $\kappa - C/L$, and much more likely to behave as $\kappa - C'/\sqrt{L}$. Convergence problems encountered in computational cells with very long aspect ratios $L_{\parallel}/L_{\perp}$ are also analyzed.

I. INTRODUCTION

Molecular dynamics (MD) simulation applies to insulating solids at high temperature T. If $k_B T$ is reasonably high on the scale of the lattice energies $\hbar\omega$, classical Newtonian trajectories give good thermal averages. Going beyond harmonic lattice dynamics is difficult with quantum mechanics, but easy with MD, not requiring perturbation theory. A "direct" simulation of thermal conductivity κ by non-equilibrium molecular dynamics (NEMD) was first done by Payton *et al.*[1] in 1967, and is now common. Good examples are the comparative study by Schelling *et al.*[2] and the careful study of GaN by Zhou *et al.*[3]. A difficulty occurs because small ω_Q vibrational modes have long mean free paths Λ_Q, but only modes with $\Lambda_Q < L$ (where L is the length of the simulation cell) have their contribution to κ correctly treated by NEMD.

Long mean free paths implies non-locality of κ. Phonons passing through point x have no information about the temperature $T(x)$, only memory of $T(x')$ where they had their previous collision. Non-locality is widely acknowledged[4–8], but not always considered a direct topic of study. Recent interest in inhomogeneous situations with boundary effects and spatially varying heat input $H(\vec{r})$ gives new impetus to non-local analysis[9–15]. Homogeneous systems are much simpler; non-locality is easy to include theoretically. A non-local analysis has value that deserves recognition.

───────

[a)]Electronic mail: philip.allen@stonybrook.edu
[b)]Electronic mail: yerong.li@outlook.com

In NEMD simulation (NE means non-equilibrium, and MD means molecular dynamics), heat $H(x)$ is added and subtracted in equal amounts ($\int dx H(x) = 0$) at different places x. After steady state is achieved, the temperature $T(x)$ is found by averaging over finite discrete sections. Usually the aim is to extract a value of dT/dx from a place distant from sources and sinks of heat. This yields a value $\kappa_{\text{eff}}(L)$ for the thermal conductivity, L being the size of the system. The result is then studied as a function of L, to extract the bulk limit $\kappa = \kappa_{\text{eff}}(L \to \infty)$. If heating $|H(x)|$ is weak, response is linear, and the relation $\Delta T(x) = \int dx' S(x - x') H(x')$ must hold. In Fourier variables, this is $\tilde{\Delta}T(q) = S(q)\tilde{H}(q)$. Using energy conservation $dJ(x)/dx = H(x)$ and the non-local Fourier law[16] $J(x) = -\int dx' \kappa(x-x') dT(x')/dx'$, we find $\tilde{\kappa}(q) = 1/q^2 S(q)$.

The procedure normally used in NEMD is to compute dT/dx at the midpoint between heat injection and removal, and thus estimate the bulk κ as the ratio of J (the current known from heat input and energy conservation) to $-dT/dx$. We denote κ derived in this way as $\kappa_{\text{eff}}(L)$, where L is the size of the system. In this paper, we show that we can do better than $\kappa_{\text{eff}}(L)$ by thinking non-locally. We show that the results of NEMD calculations can be considered to arise from $\tilde{\kappa}(q)$ for values $q = 2\pi n/L$ (for periodically repeated slabs), or $q = \pi n/L$ (for terminated slabs). Here L is the length of the simulation cell. The aim of such calculations, the true bulk $\kappa = \tilde{\kappa}(q \to 0) = \int d\vec{r}\kappa(\vec{r})/V$, requires extrapolation. This extrapolation is best guided by theory aimed at $\tilde{\kappa}(q)$. A useful strategy is therefore direct computation of $\tilde{\kappa}(2\pi/L)$, using this to optimize the extrapolation to $L \to \infty$. The reason why $\kappa = \tilde{\kappa}(0)$ is unavailable is be-

cause $\tilde{H}(0) = \int d\vec{r} H(\vec{r})/V$ must vanish in order for a steady state to be allowed.

This paper does four things. (1) We Fourier-analyze the common version of NEMD where the system is periodic with length L along the direction of heat flow, and heat input and removal occurs in isolated slabs separated by $L/2$. A rigorous relation between $\kappa_{\text{eff}}(L)$ and $\tilde{\kappa}(q)$ is worked out. (2) A method is given for direct MD simulation of $\tilde{\kappa}(q)$, by applying and extracting heat in a sinusoidal pattern[17]. This has numerical advantages over other protocols. (3) Convergence of $\tilde{\kappa}(q)$ towards κ is studied by NEMD simulation for the Lennard-Jones (LJ) liquid and crystal. (4) The Peierls "Boltzmann Transport Equation" (BTE)[18,19] is solved for $\tilde{\kappa}(q)$ in Debye approximation ($\omega_Q = v|\vec{Q}|$) with $1/\tau_Q = (1/\tau_D)(\omega_Q/\omega_D)^p$. The appropriate power p is probably 2. This helps understand convergence as the MD simulation-cell size L increases. For the particular case $p = 2$ most often encountered, it is shown that $\kappa_{\text{eff}}(L) \sim \kappa - C'/\sqrt{(L)}$, rather than the form $\sim \kappa - C/L$ which has been widely assumed.

II. PRELIMINARIES

This paper assumes a homogeneous single crystal, represented by a simulation cell with periodic boundary conditions. The ith atom at $\vec{r}_i$ and the atom at $\vec{r}_i + \vec{R}$ are equivalent, and have the same trajectory $\vec{r}_i(t)$. For simplicity, the primitive translation vectors $\vec{R}$ of the simulation cell ($\vec{A}_1$, $\vec{A}_2$, $\vec{A}_3$), are assumed orthogonal. For example, in the sample calculations presented later, they are taken to be $N_x a\hat{x}$, $N_y a\hat{y}$, $N_z a\hat{z}$, where a is the lattice constant, the edge-length of the *fcc* conventional cube. A typical cell has size $(N_x, N_y, N_z) = (80, 6, 6)$; with 4 atoms in the conventional cube, this means 11,520 atoms. Heating is done in slabs perpendicular to the long vector $\vec{A}_1$. Therefore, current flows parallel to $\vec{A}_1$, and $L = L_x = |\vec{A}_1| = N_x a$ is chosen as large as computation permits, trying to surpass the distance Λ of non-local thermal memory.

Boundaries create challenging problems. Nanoscale heat transfer is typically dominated by thermal boundary (or Kapitza) resistance[20,21]. For study of bulk conductivity, the aim is to reduce the influence of boundaries. One can argue[22] that periodic boundary conditions are not the most favorable way to do this. However, in this paper, periodicity offers simplicity for analysis, overruling other considerations.

A further simplification follows computational necessity, and discretizes the temperature $T(\vec{r})$ into slab values $T(\ell)$. The slabs are layered in the $\vec{A}_1$-direction, and have width $d = n_S a$ where n_S is a small integer and a factor of N_x. The number of slabs is $N_S = N_x/n_S$. Let the variable x denote distance along the $\vec{A}_1$-axis, perpendicular to slabs. The slab indexed by the integer ℓ occupies the interval $\ell d - d/2 < x < \ell d + d/2$. The temperature $T(\ell)$ is found from the average kinetic energy of the atoms in the ℓ'th slab. Heat is transferred externally into the ℓ'th cell at a volume-average rate $H(\ell)$. In steady state, this is balanced by an outward flux $[J(\ell+1/2) - J(\ell-1/2)]/d$. Both current and temperature gradient are properties of the junction of two adjacent slabs. Their steady-state linear relation is $J(\ell+1/2) = -\sum_{\ell'} \kappa(\ell, \ell')\nabla T(\ell'+1/2)$, where the sum runs over the N_S slabs. This definition is required by linear math. Periodicity requires $\kappa(\ell, \ell') = \kappa(\ell + mN_S, \ell' + nN_S)$ and homogeneity (if the medium is in fact homogeneous) requires that $\kappa(\ell, \ell') = \kappa(\ell - \ell')$. Corresponding (*via* a unitary Fourier transformation) to the N_S distinct slabs, there are N_S distinct wave-vectors $q_n = 2\pi n_q/N_S d = 2\pi n_q/L$, indexed by integers n_q and distributed in a one-dimensional Brillouin zone. In the homogeneous case, the relation is $\tilde{J}(q) = -\tilde{\kappa}(q)\tilde{\nabla}T(q)$. The tilde on top of a function indicates that it is in reciprocal space rather than coordinate space. These ideas were introduced in Ref. 17, where further properties are explained.

It is not hard to extend the usual derivation of the Kubo formula (ref. 23, for example) to derive a Kubo formula for $\kappa(x, x')$ or $\kappa(\ell, \ell')$. The classical limit is

$$\kappa(\ell, \ell') = -\frac{1}{k_B T^2} \int_0^\infty dt < J(\ell+1/2, t)J(\ell'+1/2, 0) > \tag{1}$$

III. DISCRETE SLAB HEATING

A common version of NEMD simulation removes energy only from slab $\ell = 0$, at a volume-average rate H, and inserts energy at the same rate into slab $\ell = N_S/2$. Zhou *et al.*[3] did a careful study of κ for GaN by this method. They discuss, but do not completely resolve, the issue of how the answer for κ scales with system size. Here we analyze this version with periodic boundaries ($\ell = \ell + N_S$), rather than the rigid or free boundaries sometimes used. Heat current $J_x(\ell+1/2) = \pm(d/2)H \equiv \pm J$ flows across slab boundaries, the plus sign for ℓ to the right of the input and left of the output slab, and the minus sign for opposite cases. Thermal conduction is found using the relation $\kappa_{\text{eff}}(L) \equiv -J/\nabla_x T(\text{mid})$. The rigorous non-local Fourier law is $\tilde{J}(q_n) = -\tilde{\kappa}(q_n)\tilde{\nabla}T(q_n)$ in the one-dimensional discrete Fourier space $q_n = 2\pi n_q/L$. Analysis given in Appendix B shows that

$$\frac{1}{\kappa_{\text{eff}}(L)} = \frac{2}{N_S} \sum_q^{n_q=\text{odd}} \frac{(-1)^{(n_q-1)/2}}{\sin(qd/2)} \left[\frac{\cos(qd/2)}{\tilde{\kappa}(q)} \right] \tag{2}$$

where the subscript on q_n has been dropped. This holds if $N_S/4$ is an integer. If it is a half-integer, then $\cos(qd/2)$ is replaced by 1. Liquids have a very local conductivity, where $\tilde{\kappa}(q) \approx \kappa$ is nearly independent of q. Then the sum in Eq.(2) converges correctly to $\kappa_{\text{eff}} \to \kappa$ without needing a small $q_1 = q_{\text{min}} = 2\pi/L$. For crystals like GaN, where non-local behavior is caused by long mean free paths of small-Q phonons, $\tilde{\kappa}(q)$ peaks around $|q| = 0$.
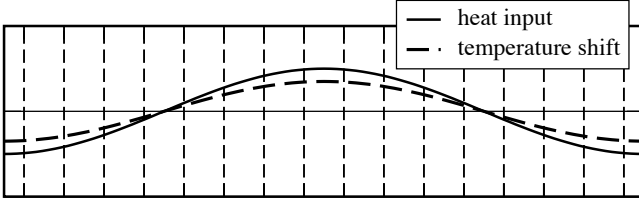
FIG. 1. Schematic picture of an $N_S = 16$ slab simulation cell with periodic boundary conditions. Heat is added or subtracted according to position, in the ℓth slab, as $H \cos(2\pi\ell/N_S)$. The central cell is numbered $\ell = 0$. Temperature $T(\ell)$ is determined by averaging kinetic energy of atoms in each slab. In linear approximation, the steady-state temperature must vary as $T_0 + \Delta T \cos(2\pi\ell/N_S)$.

Accurate results require a small $q_{\min}$ or a large L. When $q_{\min}$ is not very small, the first two terms $n_q = \pm 1$ in Eq.(2) dominate. Approximating $\sin(q_{\min}d/2)$ by π/N_S and $\cos(q_{\min}d/2)$ by 1, the result is $\kappa_{\text{eff}} \approx \pi\tilde{\kappa}(q_{\min})/4$, which is smaller than $\pi\kappa/4$ (and still smaller than the true κ.) It would be better to calculate $\tilde{\kappa}(q_{\min})$ directly. A method is given in the next section.

IV.   SINUSOIDAL HEATING ALGORITHM

The simulation cell is divided into slabs centered at $x(\ell), \ell = 1, \ldots, N_S$. It is shown schematically in Fig. 1. We want to modify the heat input profile. Instead of the two slab version, let the heat input be of the form $H(\ell) = \tilde{H}(q_{\min}) \cos(q_{\min}x(\ell))$. The temperature variation then has the form $T(\ell) = T_0 + \tilde{\Delta}T(q_{\min}) \cos(q_{\min}x(\ell))$. Since slab temperatures $T(\ell)$ at all N_S values of ℓ are used to compute the Fourier amplitude $\tilde{\Delta}T(q_{\min})$, numerical noise averages out faster.

Equation 26 of the previous paper[17] says, for arbitrary heating $H(\ell)$, heating rate, temperature, and conductivity in Fourier space are related by (for $q \neq 0$),

$$\tilde{\Delta}T(q) = \frac{\tilde{H}(q)d^2}{4\sin^2(qd/2)\tilde{\kappa}(q)} \qquad (3)$$

For simple sinusoidal heating, $\tilde{H}(q)$ and $\tilde{\Delta}T(q)$ are zero except at $q = q_{\min}$, where their values are denoted as H and ΔT. Then the conductivity is

$$\tilde{\kappa}(q_{\min}) = \frac{Hd^2/\Delta T}{4\sin^2(q_{\min}d/2)} \to \left(\frac{N_S d}{2\pi}\right)^2 \frac{H}{\Delta T} \qquad (4)$$

This makes sense: $2\pi\Delta T/N_S d$ is the maximum temperature gradient, and $HN_S d/2\pi$ is the maximum heat current.

Now we need a good numerical algorithm to drive the oscillatory heat input. Furtado et al.[24] have a nice modification of the popular algorithm by Müller-Plathe[25]. The usual Müller-Plathe method gives equal heating and

cooling to two chosen slabs, normally repeated always on the same two slabs. The hottest atom in the slab chosen for heat removal, and the coldest atom in the slab for heat insertion, have their velocities interchanged, conserving energy and momentum. The Furtado version does not interchange velocities. Instead, it adds a $\Delta\vec{v}$ to one of the two atoms, and subtracts it from the other, in such a way that energy and momentum are still conserved. The minimum possible magnitude $|\Delta\vec{v}|$, is chosen, so that the resulting disruption is minimized. This allows heat input at a predetermined rate which can be spatially varied. Appendix C gives details.

V.   TEST ON LENNARD-JONES LIQUID

The LJ liquid is a simple case, used by Müller-Plathe[25] to test his algorithm. The pair potential is

$$V_{\text{LJ}} = 4\epsilon \left[\left(\frac{\sigma}{r}\right)^{12} - \left(\frac{\sigma}{r}\right)^6 \right] \qquad (5)$$

The parameters for argon[26] are $\epsilon/k_B = 119.6$K and $\sigma = 3.405$Å. First, we reproduce Müller-Plathe's results, at the same $(N, V, T) = 2592$ atoms, $\rho = N/V = 0.849/\sigma^3$, and $T = 0.7\epsilon/k_B = 84$K. The same simulation cell is used, consisting of $20 \times 6 \times 6$ fcc conventional cubes, and periodic boundary conditions. The cut-off distance for the LJ potential is 3.0σ. We get the same answer, $\kappa = 7.1$ in LJ units.

As shown in Fig. 2 of ref. 25, and confirmed by our calculation in Fig. 2, the temperature gradient is essentially constant all the way to, and including, the slabs 0 and $N_S/2 = 10$. This is because thermal conductivity in a liquid is very local. This can be contrasted with Fig. 2 of ref. 3 or Fig. 4 of ref. 17, for crystals with non-local κ. Gas theory is certainly not correct for a liquid; the concept of a mean-free path is not valid. However, we can get an idea of what happens by unlicensed use of the gas formula $\kappa = C\bar{v}\Lambda/3$. The measured thermal conductivity of liquid argon (0.132 W/mK at temperature near 100K and pressure near 1Mbar[27–30]) then corresponds to a mean free path $\Lambda \approx 0.14$ Å, more than 30 times smaller than the slab separation $a = 1.68\sigma$. In other words, the non-local conductivity $\kappa(z-z')$ decays to zero by the first neighbor slab, or $\kappa(q)$ is independent of q out to values of q larger than $q_{\max} = \pi/d$.

Also shown in Fig. 2 is the sinusoidal temperature profile gotten numerically from our sinusoidal heating. The computational system is unaltered. The 2592 atoms are in the same cell, divided into 20 slabs, at the same T. Heat $H(\ell) = H \cos(2\pi\ell/N)$ was inserted, with H between 1 and 5 $\epsilon/(\Delta t \cdot \text{slab})$. Slabs were heated by choosing "adjoint" slabs (ℓ and $\ell + N/2$), finding coolest and hottest atoms, and altering the kinetic energies sinusoidally. This was done for all slabs simultaneously, at a fixed time step ($\Delta t = 15\delta t$ for short samples and $60\delta t$ for long samples). The time step δt used for the "velocity Verlet" Newton's-law integration algorithm[31,32]
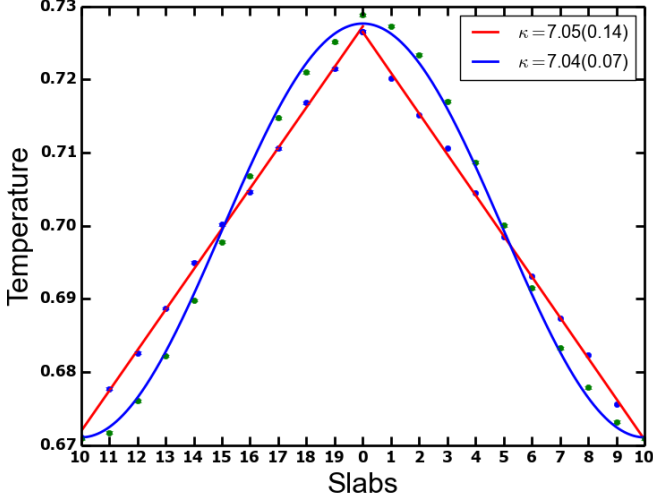
FIG. 2. Temperature profiles from NEMD simulations for the LJ liquid. The points fit by the straight line are a reproduction of the calculation of Müller-Plathe. The points fit by the sine curve use the same simulation cell, with spatially sinusoidal heating and cooling.

FIG. 3. Time evolution of the error of simulation of κ for the LJ liquid. The upper and noisier curve uses the method of Müller-Plathe. The lower curve is the result of the sinusoidal algorithm of this paper.

is $\delta t = 0.007 t_{LJ}$. The LJ unit of time for argon is $t_{LJ} = \sigma \sqrt{(m/\epsilon)} = 2.16$ ps. Equilibration required $10^4 \, \delta t$ of constant T simulation, and $T(\ell)$ averaging was done for $2 \times 10^5 \delta t$; good convergence was found in $5 \times 10^4 \delta t$ as shown in Fig. 3.

To estimate errors, consider that there are 130 atoms per slab, each with mean energy $k_B T$ and rms deviation of $k_B T$ from the mean, according to Maxwell-Boltzmann statistics. Thus the mean slab energy per atom, at any particular moment, should be about $k_B T \pm k_B T / \sqrt{130}$ Therefore, if averaged over 100 random and independent thermalized configurations, the temperature error in a slab will be less than 1%. A run of $5 \times 10^4 \delta t$ should be more than sufficient for this purpose. Fig. 2 suggests errors of order $0.001 k_B T$ in the slab temperatures.

Compared with the Müller-Plathe[25] result, both of the current ones give the same value, $\kappa = 7.1$ in LJ units, which is 0.133 W/mK, very close to the experimental value for argon, 0.132 W/mK[27–30]. The sinusoidal algorithm gives faster convergence and a slightly more accurate final answer, as shown in Fig 3.

VI. EXTRAPOLATION

NEMD answers for κ are computed for finite size L. Therefore extrapolation is required to estimate the bulk ($L \to \infty$) answer. Sellan et al.[33] have analyzed this. It was also analyzed in the previous paper[17], using a Debye model. Here we continue the analysis. Equations (22,23) of ref. 17 are

$$\kappa(q) = \frac{1}{\Omega} \sum_Q \hbar \omega_Q \frac{\partial n_Q}{\partial T} v_{Qx}^2 \tau_Q \cos^2(qd/2) F(q, \Lambda_{Qx}) \quad (6)$$
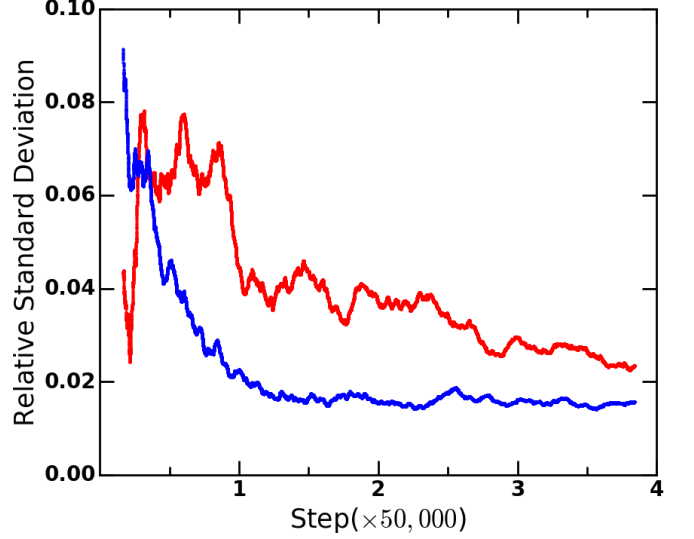
$$F(q, \Lambda) = \left[1 + 4\sin^2(qd/2) \left\{ \left(\frac{\Lambda}{d} \right) + \left(\frac{\Lambda}{d} \right)^2 \right\} \right]^{-1}, \quad (7)$$

where v_{Qx}, τ_Q, and $\Lambda = v_{Qx} \tau_Q$ are the group velocity, quasiparticle lifetime, and x-component of mean free path of the phonon mode of frequency ω_Q. The sum over modes Q implicitly includes a sum over branches. These equations solve the BTE in relaxation-time approximation (RTA; also known as the "Single Mode Approximation") for the case where heat is applied as $H(\ell) \propto \cos(q \ell d)$. We focus on the smallest q, $2\pi/L$.

Recent progress in numerical solution of the BTE[34–37] has enabled comparison of RTA against exact solutions. Very often, RTA answers are accurate at room temperature, graphene[38,39] being a notable exception. Here we adopt both the RTA and the overly simplistic Debye model. The aim is not an accurate κ, only insight about the size-dependence of $\kappa(q_{\min} = 2\pi/L)$, to guide extrapolation to the $L \to \infty$ limit. We choose the mean free path Λ_{Qx} to scale as Q^{-p},

$$\Lambda_{Qx} = v \tau_D \frac{Q_x}{Q} \left(\frac{Q_D}{Q} \right)^p. \quad (8)$$

Then Eqns.(6, 7) become

$$\kappa_D(q) = \kappa_0 \cos^2(qd/2) \frac{1}{N} \sum_Q^{3N} \left(\frac{Q_x}{Q} \right)^2 \left(\frac{Q_D}{Q} \right)^p F(q, \Lambda_{Qx}). \quad (9)$$

Here the sum over Q contains an explicit factor of 3, for the three acoustic branches, all given the same velocity v in the Debye model; κ_0 is a convenient scale factor,

$$\kappa_0 = \frac{1}{\Omega_{\text{cell}}} k_B v^2 \tau_D, \quad (10)$$

where $\Omega_{\text{cell}} = \Omega/N$. The Debye wavevector has its usual value, $(6\pi^2 N/\Omega)^{1/3}$. A common choice for the exponent is $p = 2$.

Here, instead of integrating over the Debye sphere, we use direct numerics to do the discrete sum of Eq. 9 over the actual discrete Q-mesh in the Brillouin zone of the *fcc* simulation cell that will be used in the next section for the LJ crystal. That is, we use only those $\vec{Q}$'s in the *fcc* Brillouin zone such that $\exp(i\vec{Q} \cdot \vec{A}_i) = 1$, where $\vec{A}_i$, for $i = 1, 2, 3$, are the orthogonal translation vectors of the simulation supercell. As an example, the mesh used in Sec. V for the LJ liquid corresponds to $\vec{A}_1 = 18a(1, 0, 0)$, $\vec{A}_2 = 6a(0, 1, 0)$, and $\vec{A}_3 = 6a(0, 0, 1)$, where $a = 1.68\sigma$ is the lattice constant of the *fcc* conventional cubic cell, using the liquid argon density, $0.849/\sigma^3$. Our simulation cells in this and the next section will be very similar, but longer in the $\vec{A}_1$ direction, and with a readjusted to 1.56σ to give the higher density[32,40], $1.053/\sigma^3$, of the low pressure LJ crystal. The corresponding $\vec{Q}$'s are the vectors $\ell\vec{G}_1 + m\vec{G}_2 + n\vec{G}_3$ of the lattice reciprocal to the $\vec{A}$'s. This is an anisotropic reciprocal-space mesh, being coarse in the directions $\vec{A}_2$ and $\vec{A}_3$, but finer in the direction $\vec{A}_1$, corresponding to the actual distribution of normal modes of the atoms in the simulation cell of the LJ crystal (where $|\vec{G}_{2,3}|$ is larger than $|\vec{G}_1|$.) We are guessing that the Debye model, with frequency $\omega_Q = v|\vec{Q}|$ for all 3 branches, and $1/\tau_Q = (1/\tau_D)(Q/Q_D)^2$, sufficiently captures the physics of the LJ crystal for purposes of learning how to extrapolate to infinite simulation cell size.

Results are shown in Fig. 4 and in appendices D, E, and F. The figure shows two things. First, quite smooth extrapolation to the correct $q = 0$ answer appears when $\kappa(q)$ is plotted *versus* $\sqrt{qa}$, as anticipated in Refs. 33 and 17, and clarified in Appendix D. Second, an unexpected divergence (of the form $1/\sqrt{qa}$ begins to appear for cells with small enough q (relative to the transverse size $q_\perp \approx 2\pi/N_{y \text{ or } z}$.) Specifically, the onset of the upward turn appears roughly when $\sqrt{qa} < 1/2N_y$, which corresponds to $N_x > 25N_y^2$, a limit not always achieved in NEMD calculations. The origin and significance of this divergence is discussed in Appendix E. The idea for extrapolation is discussed in the caption to Fig. 4 and in Appendix F.

VII. LENNARD-JONES CRYSTAL

Unlike the LJ liquid, for an LJ crystal, phonon gas theory applies well, but only up to half the melting temperature, where higher-order anharmonic terms become important[15]. This non-Boltzmann regime is where an MD simulation is worth doing . The resulting shorter phonon mean free paths permit shorter simulation cells. We simulate crystalline LJ argon at T=80K, close to the experimental triple point (84K and 0.7 atmospheres) and atmospheric pressure melting temperature (84K).

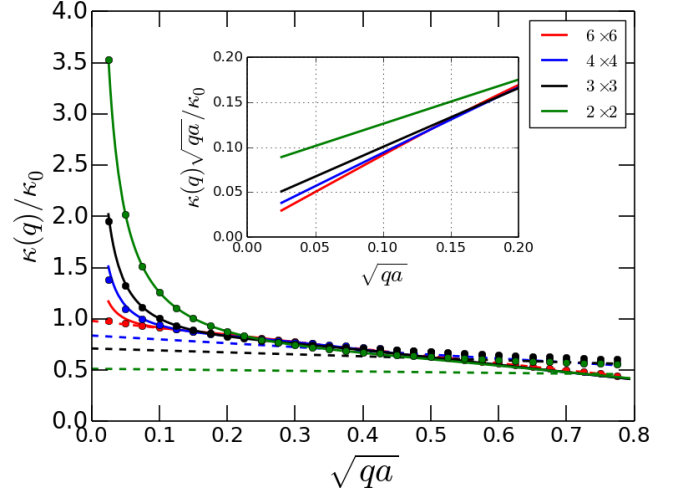Higher energy phonons have mean free paths a bit

FIG. 4. Convergence of $\kappa(q)$ toward κ_0 found by numerical summation of the Boltzmann-Debye RTA model for an anisotropic cell of size $N_y = N_z$ equalling 2, 3, 4, and 6 (top to bottom) and $N_x = 2\pi/qa$ varying from 10 to 10,000. The Q-sum in Eq.(9) is evaluated not over the Debye sphere, but over the anisotropic Q-mesh corresponding to the normal modes of the *fcc* crystalline LJ lattice; results are shown as solid lines. The inset shows that the small q divergence has a $1/\sqrt{qa}$ form with coefficient diminishing as N_y increases. The simulation results are fitted (for $50 < N_x < 1000$ or $.08 < \sqrt{(qa)} < .35$) to a 3-term form $\kappa(q) \approx A/\sqrt{(qa)} + B + C\sqrt{(qa)}$. The fits are indicated by dots whose colors agree with the lines. The value of B (for $N_x \geq 6$) is a reasonable choice for $\kappa(q = 0)$. The dashed lines show the non-diverging parts $\kappa(q) \approx B + C\sqrt{(qa)}$ of the 3-term fits. The coefficient B is the slope of the lines in the inset, and the $\sqrt{(qa)} = 0$ intercept of the dashed lines on the main graph.

longer than the unit cell $a = 5.32\mathring{A}$, which we choose to be the slab thickness d. Lower energy phonons have mean free paths Λ_Q increasing, roughly as $1/\omega_Q^2$. The values of Λ_Q are not as long as in GaN, modeled by Zhou *et al.*[3]. Nevertheless, doing a converged calculation by MD methods is challenging. We use this to test whether our algorithm is helpful. We use a time step of the "velocity Verlet" Newton's-law integration algorithm[31,32] $\delta t = 0.007t_{LJ}$ for smaller-size samples, and $0.014t_{LJ}$ for larger ones.

Figs.5 and 6 show results for $\kappa(q = 2\pi/L)$ where $L = N_x d$ is the length of the simulation cell, and $d = a$. These calculations use a heat input $H(\ell)\Delta t$ (per slab) of $1.265\epsilon \cos(2\pi\ell/N)$. The interval Δt between heat insertions is $60\delta t$. The value of κ in argon at T =80 K is measured[41] to be in the range 0.4 to 0.6 W/mK. Christen and Pollack[42] found $\kappa(80K) \approx 0.30$ W/mK. Fig. 5 looks as if it might extrapolate linearly in the region $qa < 0.1$ to a value around 23 in LJ units, whereas Fig. 6 seems more convincingly linear in $\sqrt{(qa)}$, extrapolating to a value $\kappa(q = 0) \approx 26$ in LJ units. The LJ unit of thermal conductivity is $(k_B/\sigma^2)\sqrt{(\epsilon/M)}=0.0188$ /W/mK.
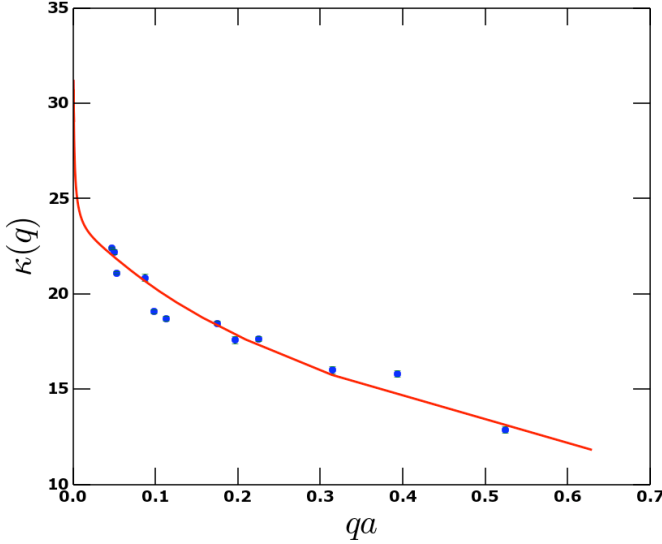
FIG. 5. Points are results of NEMD for the LJ crystal. Values of κ are shown in LJ units ($\kappa_{LJ} = (k_B/\sigma^2)\sqrt{(\epsilon/M)}$= 0.0188 W/mK). The wave-vector $q = 2\pi/L_x$ is the smallest compatible with the simulation cell, whose size is $(L_x = N_x a) \times 6a \times 6a$. Values of N_x vary from 12 to 120. The red line is a numerical summation of the Debye-RTA model, Eq. 9, using a Q-mesh compatible with the discrete normal mode quantum numbers of the y, z size of the simulation cell, and $N_x = 2\pi/qa$ values varing from 10 at the right, up to 10^4 at the left. The parameters κ_0 and τ_D are scaled to fit the NEMD numbers. The anomalous small-q behavior is better seen in Fig. 6, and is shown in Appendix E to be an artifact of the coarse $N_{y,z}$ mesh.
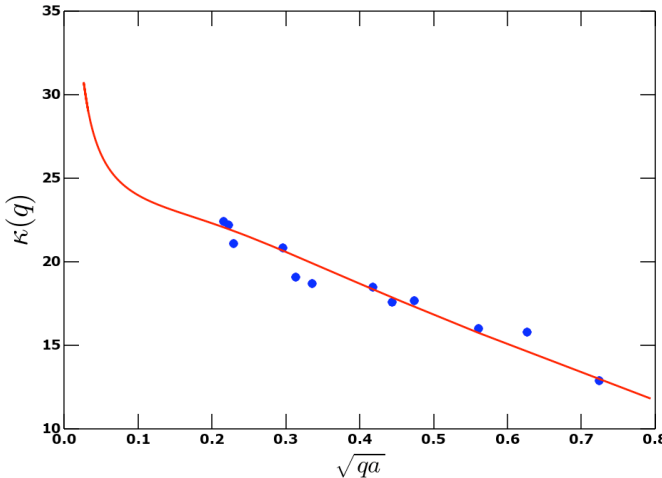

FIG. 6. Points are numerical $\kappa(q)$ in LJ units, the same as those in Fig. 5. The red line is also as in Fig. 5, a scaled RTA-Debye model with $p = 2$ (Eq. 9) summed using the same coarse transverse Q-mesh as the simulation cell, and varying N_x and thus $q = q_{min} = 2\pi/L = 2\pi/N_x a$. Use of $\sqrt{(qa)}$ for the horizontal coordinate gives better linearity and a more reliable extrapolation to $q = 0$. The anomalous low-q behavior of the red line is discussed in Appendix E.

Our LJ crystal simulation thus gives $\kappa \approx$ 0.49 W/mK. This compares with the value $0.16 - 0.17$ W/mK found by Turney *et al.*[15], 0.236 W/mK found by Omini and Sparavigna[34], 0.25 W/mK found (at 69.2K) by Kaburaki *et al.*[43], $0.33 - 0.49$ W/mK (depending on density) found by Christen and Pollack[42], and 0.19 W/mK found by Chernatynskiy and Phillpot[44].

VIII.   CONCLUSIONS

The algorithm of Sec. IV works smoothly and converges more rapidly than the common two-slab heating. It generates a reliable value of $\kappa(q = 2\pi/L)$. The macroscopic conductivity, $\kappa = \text{Lim}_{q \to 0} \kappa(q)$, found by extrapolating the long sample dimension to $L \to \infty$, is problematic, although less so than for the discrete-slab heating algorithm. Even if Boltzmann transport theory fails because phonon mean free paths are so short that quasiparticles are not well-defined, nevertheless, Boltzmann theory should correctly model the long-wavelength phonon contribution to $\kappa(q)$, which is the problematic part.

Our analysis using the BTE reveals two effects responsible for slower than expected convergence of $\kappa(q)$ to κ. These are an inevitable correction which scales as $\sqrt{(qa)}$, and the anisotropic mesh artifact that scales as $1/[N_y N_z \sqrt{(qa)}] \propto \sqrt{(N_x)}/N_y N_z$. These are found by numerical summation of the Boltzmann-Debye RTA version, but should faithfully model the effects seen in NEMD models. Simple graphical extrapolation to $q = 0$ by assuming linear behavior in $\sqrt{qa}$ is less justifiable than had been hoped, because the contamination by the $1/\sqrt{(qa)}$ term alters the appearance of the $\kappa(q)$ *versus* $\sqrt{(qa)}$ graph. The cure is to be sure that the ratio $\sqrt{(N_x)}/N_y N_z$ does not get too small. Appendix F discusses this further. There are reasons for mild insecurity on the issue of to what extent extrapolation is justified.

Appendix A: Peierls-Boltzmann-Debye (PBD) models

The normal Debye model visualizes three acoustic branches of normal modes Q. For simplicity, they are all given the same velocity v, and remain dispersionless throughout the sphere of radius Q_D which models the Brillouin zone. For anharmonic scattering, the relaxation rate $1/\tau_Q$ is Q-dependent. An appropriate extension of the Debye model is to take $1/\tau_Q = 1/\tau_D (Q/Q_D)^p$, where the power p is important but a bit uncertain in reality. The result is a family of Peierls-Boltzmann-Debye relaxation-time approximations (PBD-RTA).

$$\tilde{\kappa}_p(q) = \frac{9}{2}\kappa_0 \int_0^1 dx x^2 \int_{-1}^1 d\mu \frac{\mu^2}{x^p + i\lambda\mu} \quad (A1)$$

where $\lambda = qv\tau_D = q\ell_{min}$, and Q is the phonon mode label. The integration is over $x = Q/Q_D$, and $\mu = \cos\theta =$
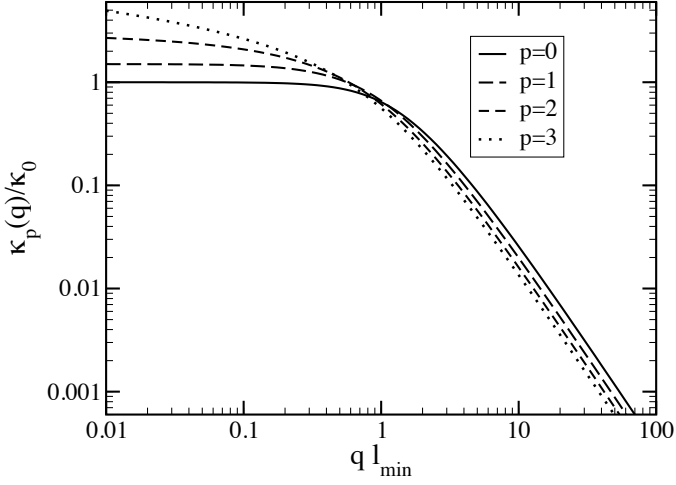
FIG. 7. The q-dependent PBD-RTA conductivities $\tilde{\kappa}_p(q)$ as expressed in Eqs.A2 to A5.

x/r. The scale factor is $\kappa_0 = k_B v^2 \tau_D / \Omega_{\text{cell}}$. This equation is just Eq.(13) of Ref. 45. It is also the continuum version ($qd \to 0$) of the discrete slab Eq. 6.

For integer p, the integrations can be done analytically:

$$\frac{\tilde{\kappa}_0(q)}{\kappa_0} = \frac{3}{\lambda^2}\left[1 - \frac{\tan^{-1}(\lambda)}{\lambda}\right] \qquad (A2)$$

$$\frac{\tilde{\kappa}_1(q)}{\kappa_0} = \frac{9}{10}\left[1 + \frac{2}{\lambda^2}\left(1 - \frac{\tan^{-1}(\lambda)}{\lambda}\right) - \lambda^2\log\left(1 + \frac{1}{\lambda^2}\right)\right] \qquad (A3)$$

$$\frac{\tilde{\kappa}_2(q)}{\kappa_0} = \frac{9}{7\lambda^2}\left[1 - \frac{\tan^{-1}(\lambda)}{\lambda} + 2\lambda^2\right.$$
$$- \lambda^2\sqrt{\frac{\lambda}{2}}\left(\tan^{-1}\left(\sqrt{\frac{2}{\lambda}} + 1\right) + \left(\sqrt{\frac{2}{\lambda}} - 1\right)\right)$$
$$\left. - \frac{\lambda^2}{2}\sqrt{\frac{\lambda}{2}}\log\left(\frac{1 + \sqrt{2\lambda} + \lambda}{1 - \sqrt{2\lambda} + \lambda}\right)\right] \qquad (A4)$$

$$\frac{\tilde{\kappa}_3(q)}{\kappa_0} = \frac{1}{2}\log\left(\frac{1 + \lambda^2}{\lambda^2}\right) + \frac{1}{\lambda^2}\left(1 - \frac{\tan^{-1}(\lambda)}{\lambda}\right) \qquad (A5)$$

These equations are plotted versus $\lambda = q\ell_{\min}$ in Fig.7.

These four functions have simple large-q limits,

$$\tilde{\kappa}_p(q) = \frac{9}{3 + p}\frac{\kappa_0}{(q\ell_{\min})^2}. \qquad (A6)$$

Their small-q limits are diverse, and contain the rules for extrapolation to $q = 0$. The $p = 0$ function $\tilde{\kappa}_0$ hardly requires extrapolation if the cell size significantly exceeds $\ell_{\min} = v\tau_D$. The $p = 3$ function diverges as $\log(1/q)$ to infinity as $q \to 0$. If the exponent p exceeds 3, the divergence is faster than logarithmic. The explicit formulas are

$$\frac{\tilde{\kappa}_0(q)}{\kappa_0} \to 1 - \frac{3}{5}\lambda^2 + \dots \qquad (A7)$$

$$\frac{\tilde{\kappa}_1(q)}{\kappa_0} \to \frac{3}{2} - \frac{9}{5}\lambda^2\log(1/\lambda) - \frac{9}{25}\lambda^2 + \dots \qquad (A8)$$

$$\frac{\tilde{\kappa}_2(q)}{\kappa_0} \to 3 - \frac{9\pi}{7}\sqrt{\frac{q\ell_{\min}}{2}} + \dots \qquad (A9)$$

$$\frac{\tilde{\kappa}_3(q)}{\kappa_0} \to \log(1/q\ell_{\min}) + 3 + \dots \qquad (A10)$$

For $p > 0$, the leading term is non-analytic in q, but higher corrections are analytic.

Appendix B: Discrete slab heating

Adding periodic boundary conditions permits a simple Fourier representation of J_x,

$$\tilde{J}_x(q) = \frac{1}{N_S}\sum_{\ell=0}^{N_S-1} e^{-iqx(\ell+1/2)}J_x(\ell + 1/2)$$
$$= \frac{J}{N_S}\sum_{\ell=0}^{N_S/2-1}\left[e^{-iqx(\ell+1/2)} - \text{c.c.}\right]$$
$$= \frac{J}{N_S}\left(\frac{1 - e^{-iqL/2}}{1 - e^{iqd}}\right)e^{-iqd/2} - \text{c.c.}$$
$$= \frac{J}{iN_S}\left[\frac{1 - (-1)^{n_q}}{\sin(qd/2)}\right] \qquad (B1)$$

At $q = 0$, the expression [ ] in the last line of Eq.(B1) needs definition; the correct value is 0, as is also true for all q's with even n_q. Now let us analyze the approximate thermal conductivity,

$$\kappa_{\text{eff}}(L) \equiv -J/\nabla_z T(\text{mid}). \qquad (B2)$$

That is, the thermal conductivity is approximated by the ratio of the actual current J, controlled by the heating rate $\dot{e}$, to the temperature gradient $-\nabla_z T(\text{mid})$ found midway between the heat input slab ($\ell = 0$) and output slab ($\ell = N_S/2$). This temperature gradient has the Fourier representation

$$\nabla_z T\,(\text{mid}) = \sum_q e^{iqN_S d/4}\nabla_z T(q) \quad [N_S/4 = \text{half integer}]$$
$$= \sum_q e^{iqN_S d/4}\cos(qd/2)\nabla_z T(q) \quad [N_S/4 = \text{integer}] \qquad (B3)$$

In the case $N_S/4 = $ integer, the slab $\ell = N_S/4$ lies midway between heat input and output, so the temperature gradient (needed at the slab mid-point) is taken as the average of the left and right slab boundaries. This introduces the factor $\cos(qd/2)$ in the second version of Eq.(B3). Finally, we substitute $\nabla_z T(q) = -J_z(q)/\kappa(q)$ in Eq.(B3), and use Eq.(B1) for $J_z(q)$. Then Eq.(B2)

becomes

$$\frac{1}{\kappa_{\text{eff}}} = \frac{2}{N_S} \sum_{q}^{n_q=\text{odd}} \frac{\sin(qL/4)}{\sin(qd/2)} \left[\frac{1 \text{ or } \cos(qd/2)}{\kappa(q)} \right]$$

$$= \left[\frac{4 \text{ or } 4\cos(\pi/N_S)}{N_S \sin(\pi/N_S)} \right] \frac{1}{\kappa(q_{\min})} + \{|n_q| \geq 3 \text{ terms}\}. \tag{B4}$$

This is a surprisingly complicated relation between the size-dependent "computational" value of κ_{eff} and the Fourier representation $\kappa(q)$. From Eq.(B4), the leading term (at small $q_{\min}d/2 = \pi d/L = \pi/N_S$) is $1/\kappa_{\text{eff}} = 4/\pi\kappa(q_{\min})$, with oscillatory corrections $\sum_{n=1}(4/\pi)(-1)^n/[(2n+1)\kappa((2n+1)q_{\min})]$. In the local limit, $\kappa(q) = \kappa$, Eq.(B4) converges exactly to $\kappa_{\text{eff}} = \kappa$.

Appendix C: Heat exchange algorithm

The Müller-Plathe recipe is: find the hottest atom in the cold ($\ell = N_S/2$) slab, and the coldest atom in the hot ($\ell = 0$) slab. Interchange their velocities. Energy and momentum are both conserved, and the system is driven from equilibrium in a way that must be monitored. Cao and Li[46] among others, have suggested modified algorithms of this type.

In our method, driving is done by spatially periodic injection and simultaneous removal of heat. Examine a slab ℓ (with $0 \leq \ell < N_S/4$), and its conjugate slab $N_S/2 - \ell$. The former is "hotter" than the latter because $\dot{e}(\ell) > 0 > \dot{e}(N_S/2 - \ell) = -\dot{e}(\ell)$. Find the coldest atom (meaning least kinetic energy) of all atoms of mass m_i in the hotter slab, denoting its velocity as $\vec{v}_C$. Find the hottest atom of the same mass in the colder slab, denoting its velocity $\vec{v}_H$. Given the large fluctuations of the Maxwell-Boltzmann ensemble, it is certain that $v_H^2 > v_C^2$. Choose an appropriate velocity $\vec{w}$ and add it to the velocity $\vec{v}_C$ and subtract it from $\vec{v}_H$:

$$\vec{v}_H \to \vec{v}_H - \vec{w}$$
$$\vec{v}_C \to \vec{v}_C + \vec{w} \tag{C1}$$

The same operation should be done for the pair of slabs $-\ell$ and $\ell - N_S/2$. All slabs can be done simultaneously, or different random times can be used for different slabs.

There are three criteria for an appropriate $\vec{w}$, which uniquely fix the desired choice. (i) The cold atom's kinetic energy should increase by Δ, an energy that can be specified in advance as $(\dot{e}\Omega_S\tau)\cos(2\pi\ell/N_S)$, where τ is the average time interval between random interventions, and Ω_S is the volume of a slab. (ii) The hot atom's kinetic energy should decrease by Δ. Then both momentum and energy are conserved. Heating has the desired form $\dot{e}\cos(2\pi\ell/N_S)$ with $\dot{e}$ chosen not too different from $k_B T/\Omega_S\tau$. Trial calculations should test for the best choices of $\dot{e}$ and τ. (iii) There is still a one-dimensional family of vectors $\vec{w}$; from these, choose the smallest $|\vec{w}|$, which gives the least impulse to the affected atoms.
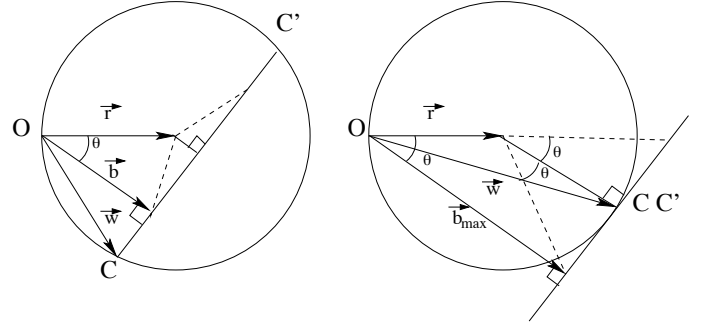

FIG. 8. Geometric construction for finding the smoothest velocity change $\vec{w}$ of the coldest atoms (with velocity $\vec{v}_C$ in the hotter region and the hottest atoms (with velocity $\vec{v}_H$ in the colder region. Both figures represent a sphere of radius $\vec{r} = (\vec{v}_C - \vec{v}_H)/2$. The plane perpendicular to $\vec{b}$, intersects the sphere in a circle, which is the locus of solutions $\vec{w}$ obeying energy and momentum conservation rules. The points C and C' (in the $\vec{r}$–$\vec{b}$ plane) give the solutions with least and greatest impulse. The right-hand version shows the largest vector $\vec{b}$ which allows solutions for $\vec{w}$. The minimum and maximum impulse solutions have merged to a point.

The energy shift criteria (i) and (ii) give equations $-2\vec{v}_H \cdot \vec{w} + w^2 = -2\Delta/m \equiv -\delta$, and $2\vec{v}_C \cdot \vec{w} + w^2 = +\delta$. Adding and subtracting these equations give

$$\delta = (\vec{v}_H + \vec{v}_C) \cdot \vec{w}$$
$$w^2 = (\vec{v}_H - \vec{v}_C) \cdot \vec{w}, \tag{C2}$$

a linear and a quadratic equation for $\vec{w}$. These have a simple geometric interpretation shown in Fig. 8. The first equation restricts the projection of $\vec{w}$ along the vector $\vec{v}_H + \vec{v}_C$. Geometrically, this means that $\vec{w}$ lies on the plane (shown by C, C' in Fig. 8) perpendicular to the vector $\vec{b} \equiv \delta(\vec{v}_C + \vec{v}_H)/|\vec{v}_C + \vec{v}_H|^2$, where the origin of $\vec{w}$ coincides with the origin of $\vec{b}$. The second equation restricts $\vec{w}$ to the surface of a sphere of radius $|\vec{v}_H - \vec{v}_C|/2$, centered at the end of the vector $\vec{r} \equiv (\vec{v}_H - \vec{v}_C)/2$, whose origin also coincides with the origin of $\vec{w}$. The sphere and the plane intersect on a circle, indicated by C, C' in Fig. 8. This circle is the one-dimensional family of solutions $\vec{w}$ satisfying Eqs.(C2). It is also clear from the geometry that the shortest vector $\vec{w}$ (the one that satisfies criterion (iii)) is the one shown, from O to C. This lies in the same plane as the two known vectors $\vec{r}$ and $\vec{b}$ (also the same plane as $\vec{v}_H$ and $\vec{v}_C$). Therefore

$$\vec{w} = \alpha\vec{r} + \beta\vec{b}$$
$$\vec{r} = (\vec{v}_H - \vec{v}_C)/2$$
$$\vec{b} = \frac{\delta(\vec{v}_H + \vec{v}_C)}{|\vec{v}_H + \vec{v}_C|^2}. \tag{C3}$$

These definitions allow Eqs.(C2) to be written as

$$b^2 = \vec{w} \cdot \vec{b}$$
$$w^2 = 2\vec{r} \cdot \vec{w}. \tag{C4}$$

The solution for $\vec{w}$ is

$$\beta = 1 - \alpha \frac{\vec{r} \cdot \vec{b}}{b^2}$$

$$\alpha = 1 - \sqrt{1 - X}$$

$$X = \frac{(b^2 - 2\vec{b} \cdot \vec{r})b^2}{b^2 r^2 - (\vec{b} \cdot \vec{r})^2} \qquad (C5)$$

To derive this, substitute Eq.(C3) for $\vec{w}$ in terms of the unknown coefficients α and β into the Eqs.(C2). The linear equation is used to find β in terms of α. Eliminating β in favor of α in the quadratic equation gives a quadratic equation for α. The appropriate solution is displayed in Eq.(C5). An alternate version directly in terms of the velocities $\vec{v}_H$ and $\vec{v}_C$ is

$$X = (2\Delta/m) \frac{(2\Delta/m) - (v_H^2 - v_C^2)}{v_H^2 v_C^2 - (\vec{v}_H \cdot \vec{v}_C)^2} \qquad (C6)$$

$$\vec{w} = \frac{\alpha}{2}(\vec{v}_H - \vec{v}_C) + \left[\frac{2\Delta}{m} - \frac{\alpha}{2}(v_H^2 - v_C^2)\right] \frac{\vec{v}_H + \vec{v}_C}{|\vec{v}_H + \vec{v}_C|^2} \qquad (C7)$$

Notice that X in Eq.(C6) has a non-negative denominator that becomes zero in an accidental event where $\vec{v}_H$ and $\vec{v}_C$ are parallel; X is then ill-defined, because no solution exists. An alternate pair of C and H atoms must be chosen. In the simulations reported in subsequent sections, we find that Δ should be chosen small, making the numerator of X in Eq.(C6) negative. Thus both X and α are negative, contrary to the version shown in Fig. 8. This does not adversely affect anything.

There is a second solution, $\alpha = 1 + \sqrt{1 - X}$, corresponding to the maximum $|\vec{w}|$, designated as C' in Fig. 8. For $|\vec{b}| > b_{\max}$, there are no real solutions. This corresponds to $X > 1$. The condition for the two solutions to coincide is $X = 1$, which agrees with $b_{\max} = r(1 + \cos\theta)$, where θ is the angle between $\vec{b}$ and $\vec{r}$. This can be understood from the right hand part of Fig. 8, illustrating the case where the circle collapses to a point. For reasonable choices of the parameter $m\delta/2 = \Delta$, meaning values smaller than or similar to $k_B T/N_S$, solutions should always exist.

Appendix D: Homogeneous Mesh

On Figs. 5 and 6, the red line shows the RTA-Debye results when numerically summed over the mesh in Q associated with the harmonic normal mode basis corresponding to simulation cells. It is interesting instead to ask what analytic answers can be extracted for the dependence of κ on simulation cell size. This can be approached in several ways. In this Appendix, a large, isotropic cell is discussed (volume $\Omega = L^3$). Finite size means that the wave vector $\vec{q}_{\min} = (2\pi/L)(0,0,1)$ is non-zero. The phonon wave-vector mesh $\vec{Q}_{\min} = (2\pi/L)(n_x, n_y, n_z)$ is therefore in principle discrete. However, a continuum

approximation works for the present purposes, because the integrand is a smooth function of $\vec{Q}$, and the singular correction term arises when only q is kept discrete. Equations 6 and 7, when combined, are

$$\kappa(q) = \frac{1}{\Omega} \sum_Q \hbar\omega_Q \frac{\partial n_Q}{\partial T} v_{Qz}^2 \tau_Q \frac{\cos^2(qd/2)}{1 + 4\sin^2(qd/2)(\Lambda/d)^2} \qquad (D1)$$

The term linear in Λ/d in the denominator of Eq. 7 was dropped because q-dependent corrections are only important when $\Lambda/d = v\cos\theta\tau_Q/d$ is large (since $\tau_Q = \tau_D(Q_D/Q)^p$ is large.) Then the quadratic term $(\Lambda/d)^2$ dominates. In classical approximation, $\hbar\omega_Q \frac{\partial n_Q}{\partial T} \to k_B$, and in Debye approximation, $v_{Qz} = v\cos\theta$. We are interested in the minimum wavevector $q = 2\pi/L$, so $\cos(qd/2) \to 1$ and $2\sin(qd/2)\Lambda/d \to 2\pi\Lambda/L$. Then Eq. D1 becomes (for the special case $p = 2$)

$$\kappa(q_{\min}) = \frac{\kappa_0}{3N} \sum_Q \frac{\cos^2\theta(Q_D/Q)^2}{1 + \cos^2\theta\lambda^2(Q_D/Q)^4} \qquad (D2)$$

where $\lambda \equiv q\ell_{\min} = 2\pi v\tau_D/L$ and $\kappa_0 = 3k_B v^2\tau_D N/\Omega$. This is the Debye-RTA result for any choice of cell dimensions (N_x, N_y, N_z) and corresponding Q-mesh. There are two parameters, $\ell_{\min}$ which determines the scale of q through the relation $\lambda = q\ell_{\min}$, and κ_0 which determines the scale of κ. In the numerical results shown in Sec. VI, Fig. 4, and later in Appendix F, Figs. 9,10,11, the choices were made $\ell_{\min} = 2.45a$ and $\kappa_0 = 26.44$ (in LJ units). These choices were made simply to scale the numerical summations to fit the numerical simulations of Sec. VII.

For a uniform and dense mesh (*i.e.* a large crystal), the sum becomes an integral,

$$\frac{1}{N} \sum_Q \to \frac{9}{2} \int_0^{Q_D} \frac{dQ Q^2}{Q_D^3} \int_{-1}^1 d\cos\theta, \qquad (D3)$$

where an extra factor of 3 is for the three modes. After performing the angular integral, D2 becomes

$$\kappa(q_{\min}) = \frac{3\kappa_0}{\lambda^2} \int_0^{Q_D} \frac{dQ Q^4}{Q_D^5}$$

$$\times \left[1 - \frac{1}{\lambda}\left(\frac{Q}{Q_D}\right)^2 \tan^{-1}\lambda\left(\frac{Q_D}{Q}\right)^2\right]$$

$$= \frac{3\kappa_0}{2\lambda^2} \int_0^1 du\, u^{3/2}\left[1 - \frac{u}{\lambda}\cot^{-1}\frac{u}{\lambda}\right]. \qquad (D4)$$

Here the replacements have been made $u = (Q/Q_D)^2$ and $\tan^{-1}(1/x) = \cot^{-1} x$.

Next we assert the following identity, best proved by

direct differentiation:

$$
\begin{aligned}
h(u) &= \frac{7}{2} \int du \left[u^{3/2} - \frac{u^{5/2}}{\lambda} \cot^{-1} \frac{u}{\lambda} \right] \\
&= u^{5/2} + 2\lambda^2 u^{1/2} - \frac{u^{7/2}}{\lambda} \cot^{-1} \frac{u}{\lambda} \\
&\quad - \frac{\lambda^{5/2}}{\sqrt{2}} \left[\frac{1}{2} \log \left(\frac{u + \sqrt{2u\lambda} + \lambda}{u - \sqrt{2u\lambda} + \lambda} \right) + \tan^{-1} \left(\frac{\sqrt{2u\lambda}}{\lambda - u} \right) \right]
\end{aligned}
$$

(D5)

Now we have an answer,

$$
\kappa(q_{\min}) = \frac{3}{7} \frac{\kappa_0}{\lambda^2} [h(1) - h(0)] \tag{D6}
$$

It is necessary to be careful in evaluating $h(1) - h(0)$. As we integrate u from 0 towards 1 (as in Eq.D4), all the terms in the integral, Eq.D5 have smooth behavior except the last term, $\tan^{-1}[\sqrt{(2u\lambda)}/(\lambda - u)]$. Note that $0 < \lambda < 1$ since L is large. Therefore, in this term, the argument of the arctangent increases from zero to $+\infty$, where the arctangent equals $\pi/2$, then switches to $-\infty$, with the arctangent still equal to $\pi/2$, and finally increases toward 0 from the negative side, with the arctangent approaching π from the negative side. Therefore, the value of $\tan^{-1}[\sqrt{(2u\lambda)}/(\lambda - u)]$ at $u = 1$ is $\pi - \tan^{-1}[\sqrt{(2\lambda)}/(1 - \lambda)]$. The answer is thus

$$
\begin{aligned}
\frac{7\lambda^2}{3\kappa_0} \kappa(q_{\min}) &= 1 + 2\lambda^2 - \frac{\tan^{-1}\lambda}{\lambda} \\
&\quad - \frac{\lambda^{5/2}}{\sqrt{2}} \left[\frac{1}{2} \log \left(\frac{1 + \sqrt{2\lambda} + \lambda}{1 - \sqrt{2\lambda} + \lambda} \right) + \pi - \tan^{-1} \left(\frac{\sqrt{2\lambda}}{1 - \lambda} \right) \right]
\end{aligned}
$$

(D7)

Finally, at large sample size L, the smallest mean free path $\ell_{\min} = v\tau_D$ is small compared with L. The parameter λ is $2\pi\ell_{\min}/L$ and the leading size-dependent correction is

$$
\frac{\kappa(q_{\min})}{\kappa_0} = 1 - \frac{3\pi}{7} \sqrt{\frac{\pi\ell_{\min}}{L}} = 1 - \frac{3\pi}{7} \sqrt{\frac{\ell_{\min}}{2a}} \sqrt{(qa)}. \tag{D8}
$$

This result confirms the conjecture of Refs. 33 and 17 that numerical result might be best extrapolated by plotting κ *versus* $\sqrt{(1/L)}$.

Appendix E: Inhomogeneous mesh

Fig. 6 indicates that the analytic answer of Eq. D8 gives a good match to the size-dependence when L_z is not too big (and q is not too small.) At smaller q there is an up-turn in the numerical Debye-RTA sum, that is not derived in the analytic integration Eq. D7. This up-turn is strongly enhanced at small transverse cell size $N_x N_y$. The problem is that the ratio L_z/L_x becomes very large at small $q = 2\pi/L_z$. It is necessary to reconsider how Eq. D1 behaves in a finite-size crystal or simulation cell, when one dimension ($L_z \equiv L$) gets large but the other two ($L_x = L_y \equiv L_{xy}$) remain small. The answer is, a new non-analytic piece occurs, and rather than converging to the $L \to \infty$ limit as $1/\sqrt{L}$ (found above for the homogeneous mesh), it diverges as $\sqrt{L}$. These results are specific to the power law relaxation $\tau_Q = \tau_D(\omega_D/\omega)^p$ with $p = 2$. The divergence is a property of a one-dimensional wire, indicating that ballistic transport has a dominant effect in such a system. As the area $L_x L_y$ of the wire increases, the divergent term in $\kappa(q_{\min})$ decreases as $a^2/L_x L_y$, restoring the better-behaved homogeneous answer.

The specific system under consideration is an fcc crystal of volume $Na^3/4$, where a is the conventional primitive cube size, $N = 4N_x N_y N_z$ is the total number of atoms, N_x and N_y being small integers held fixed, and N_z being a large integer. We seek the behavior as N_z gets very large. The conductivity is given by Eq. D2, rewritten as

$$
\frac{\kappa(q_{\min})}{\kappa_0} = \frac{1}{N} \sum_{Q_z} \sum_{Q_x,Q_y} \frac{(Q_z/Q)^2 (Q_D/Q)^2}{1 + (Q_z/Q)^2 \lambda^2 (Q_D/Q)^4}, \tag{E1}
$$

where $\lambda = 2\pi\ell_{\min}/L$, $\ell_{\min}$ being the mean free path of the highest frequency phonons. The Q-vectors are $\vec{Q} = (2\pi/a)(n_x/N_x, n_y/N_y, n_z/N_z)$. This choice is required to make vibrational normal modes satisfy periodicity in the supercell. There are N Q-vectors in the Brillouin zone. The Debye model simplifies summation over the Brillouin zone by using the Debye sphere, with a volume equal to n times the volume of the primitive Brillouin zone, n being the number of atoms in the primitive cell, 4 for fcc. The Q-points are dense along the z direction and sparse in the others. Only the Q_z-sum can be turned into an integral. It is consistent with the philosophy of the Debye model, to not use a sphere in this case, but a cube-shaped "pseudo-Brillouin zone", of volume 4 times $(2\pi/a)^3$, containing the correct number of states. The Q_z sum is then an integral, going from $Q_z = 0$ to the boundary of the "pseudo-Brillouin zone," $4^{1/3}\pi/a$, and multiplied by 2 to cover both negative and positive Q_z.

$$
\begin{aligned}
\frac{\kappa(q_{\min})}{\kappa_0} &= \frac{1}{4N_x N_y} \sum_{Q_x,Q_y} \frac{a}{\pi} \\
&\quad \int_0^{4^{1/3}\pi/a} dQ \frac{(Q_z/Q)^2 (Q_D/Q)^2}{1 + (Q_z/Q)^2 \lambda^2 (Q_D/Q)^4}
\end{aligned}
$$

(E2)

The number of terms in the Q_x, Q_y sum is $\approx n^{2/3} N_x N_y$, typically 50 for an MD simulation, or a few thousand for a small nanowire. Of these terms, the one which requires special attention is the $Q_x = Q_y = 0$ term. We denote this term by $\kappa_{00}(q_{\min})$,

$$
\begin{aligned}
\frac{\kappa_{00}(q_{\min})}{\kappa_0} &= \frac{1}{4N_x N_y} \frac{a}{\pi} \int_0^{4^{1/3}\pi/a} dQ \frac{Q^2 Q_D^2}{Q^4 + \lambda^2 Q_D^4} \\
&= \frac{(3/\pi)^{1/3}}{2N_x N_y} \int_0^{\zeta} du \frac{u^2}{u^4 + \lambda^2},
\end{aligned}
$$

(E3)

where the variable u is Q/Q_D, and the upper limit is $\zeta = (\pi/6)^{1/3}$. Using similar algebra to that of Appendix A, the answer is

$$\frac{\kappa_{00}(q_{\min})}{\kappa_0} = \frac{(3/\pi)^{1/3}}{2N_xN_y}[g(\zeta) - g(0)], \qquad (E4)$$

where the indefinite integral $g(u)$ is

$$g(u) = \frac{1}{2\sqrt(2\lambda)}\left[-\frac{1}{2}\log\left(\frac{u^2 + \sqrt{2\lambda}u + \lambda}{u^2 + \sqrt{2\lambda}u + \lambda}\right)\right.$$
$$\left. + \tan^{-1}\left(\frac{\sqrt{2\lambda}u}{\lambda - u^2}\right)\right]. \qquad (E5)$$

Because N_z is large, $\lambda = 2\pi\ell_{\min}/N_z a$ is small, and to first order, the definite integral $g(\zeta) - g(0)$ is determined by the phase of the arctangent, and equals $\pi/2\sqrt(2\lambda)$, insensitive to the details of the "pseudo-Brillouin zone" boundary location. Thus to leading order, the piece of $\kappa(q)$ coming from the $Q_x = Q_y = 0$ part of the Q-mesh, is

$$\frac{\kappa_{00}(q_{\min})}{\kappa_0} = \frac{(3/\pi)^{1/3}}{2N_xN_y}\frac{\pi}{4}\sqrt{\frac{L}{\pi\ell_{\min}}} \qquad (E6)$$

The Debye model is reliable as a guide for the low frequency behavior, provided the relaxation-time approximation and the associated power law p are correct. The conclusion is a bit surprising. It indicates that if anisotropic simulation cells are used for NEMD simulation of κ, then the extrapolation to very long cells suffers from an unintended 1D singularity. The product N_xN_y should increase at least as rapidly as $N_z^{1/2}$ to prevent this term distorting the extrapolated answer. In actual simulations, this is probably more a sobering thought than a serious warning. But the effect is real, and shows up in the Debye-model numerics shown in Figs. 5 and 6.

Appendix F: Semi-empirical Fitting

Figures 5 and 6 show (as red lines) Debye-RTA discrete Q-sums adjusted to fit NEMD results. These are intended to guide extrapolation, but reveal possible ambiguity about how to correct for the $1/\sqrt(qa)$ behavior. This is an artifact of too large a ratio N_z/N_x, not achieved in the NEMD simulations, but easily achieved in the Debye-RTA numerical sums on discrete Q-meshes. Here we show some results of a 3-term fit to the numerical Debye-RTA sums. From Appendices D and E, we are led to expect behavior of the type

$$\kappa(q)/\kappa_0 \approx A/\sqrt{qa} + B + C\sqrt{qa}. \qquad (F1)$$

The coefficient A should diminish as N_xN_y, since it arises from only the $Q_x = 0$ and $Q_y = 0$ part of the normal mode spectrum, one part out of the total of $N_xN_y Q_x$, Q_y-values. This is tested in Fig. 9, and found correct.
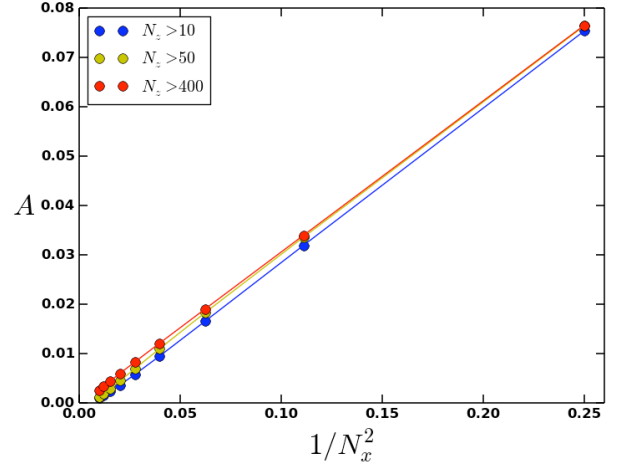

FIG. 9. The coefficient of the singular part $\propto 1/\sqrt(qa)$ scales nicely with the reciprocal of the transverse dimension $1/N_x^2$ of the simulation cell, especially when the semi-empirical fit is restricted to smaller values of q.

Numerical summation over the Q-mesh was done for 7 choices of $N_x = N_y$, namely 2, 3, 4, 5, 6, 8, and 10, and for a mesh of N_z ranging from the coarse value of 10 to the dense value of 10,000. The 7 resulting $\kappa_{\text{Debye}}(q)$ curves were least-squares fitted to Eq. F1. The fitting was done for the smallest $q = 2\pi/N_z a$, up to a cutoff (all N_z greater than a minimum value, chosen as 10, 50, or 200.) The fit is extremely accurate for the smallest q-cut ($N_z = 200$) and least accurate for the largest ($N_z = 10$.) The scaling with $1/N_x^2$ behaves just as expected. The singular up-turn at very small q is indeed an artifact of an anisotropic simulation cell, and should be avoided by not letting the ratio $N_z/(N_xN_y)$ become too large.

The coefficient B is supposed to represent the true converged $q \to 0$ limit of $\kappa(q)$. Figure 10 shows how this coefficient behaves as the transverse dimension increases. For $N_x = N_y = 10$, the Debye-RTA calculation is converged to 96% or better, no matter what range of q is used for least-squares fitting. Even down to $N_x = N_y = 5$, the value of B is 95% of the bulk value 1, provided all cell sizes down to the smallest ($N_z = 10$) are included in the least-squares fit, whereas, if only small q's ($N_z > 200$) are used, convergence is a lot slower. This odd result indicates that the improved convergence found by fitting the less relevant large q's is likely to be partially a result of a fortuitous cancellation of errors.

Finally, the leading finite size effect for bulk $\kappa(q)$ is contained in the term $C\sqrt(qa)$. This term comes long-wavelength phonons whose mean-free path exceeds the cell size unless the cell is large in all three directions. This negative contribution to κ is apparently suppressed when the cell becomes more anisotropic. Simultaneously the diverging term is getting larger. These seem to accidentally compensate, making the NEMD answers better than the true convergence estimates lead one to expect. This is nicely illustrated in Fig. 4, which shows that
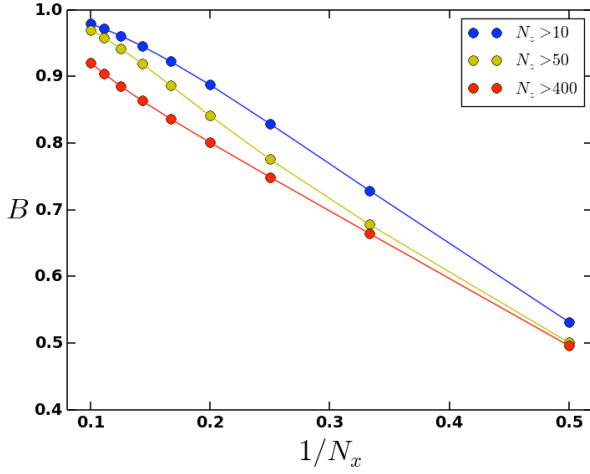
FIG. 10. The expected $q \to 0$ limit of Debye-RTA numerical sums corresponds to coefficient $B \to 1$, which happens nicely as the transverse cell size is increased to 10×10. The fact that it happens most quickly when even short cells $N_z = 10$ are included in the fit, suggests fortuitous error cancellation.
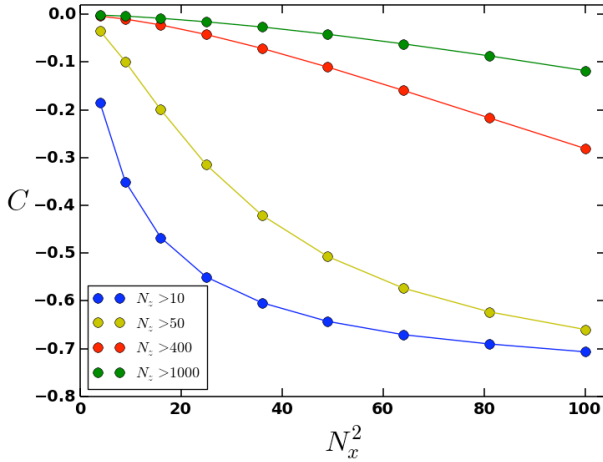

FIG. 11. The coefficient C of the leading finite size correction $\kappa(q)/\kappa_0 \approx 1 + C\sqrt{(qa)}$ is suprisingly sensitive to transverse simulation cell size and to the choice of q-range to use in the fit.

for N_z not too big ($0.22 < \sqrt{(qa)} < 0.5$, corresponding to $25 < N_z < 130$), the curve of $\kappa(q)$ *versus* $\sqrt{(qa)}$ is remarkably independent of N_x and appears to point smoothly to the correct extrapolated value of κ_0. The more careful fitting to the 3-term expression gives extrapolated values shown by the dotted lines, which converge well for meshes $N_x \geq 6$, but not as rapidly as the less careful extrapolation. The prescription for extrapolation of NEMD with realistic simulation cells seems to be, don't use meshes with $N_x = N_y$ much smaller than 6, and extrapolate linearly if numerical results appear linear when plotted against $\sqrt{(qa)} \propto 1/\sqrt{(N_z)}$.

[1] D. N. Payton, M. Rich, and W. M. Visscher, Phys. Rev. **160**, 706 (1967), URL http://link.aps.org/doi/10.1103/PhysRev.160.706.

[2] P. K. Schelling, S. R. Phillpot, and P. Keblinski, Phys. Rev. B **65**, 144306 (2002), URL http://link.aps.org/doi/10.1103/PhysRevB.65.144306.

[3] X. W. Zhou, S. Aubry, R. E. Jones, A. Greenstein, and P. K. Schelling, Phys. Rev. B **79**, 115201 (2009), URL http://link.aps.org/doi/10.1103/PhysRevB.79.115201.

[4] I. B. Levinson, Soviet Physics JETP **52**, 704 (1980), URL http://www.jetp.ac.ru/cgi-bin/e/index/e/52/4/p704?a=list.

[5] T. E. Wilson, F. M. Lurie, and W. E. Bron, Phys. Rev. B **30**, 6103 (1984), URL http://link.aps.org/doi/10.1103/PhysRevB.30.6103.

[6] U. Happek, T. Holstein, and K. F. Renk, Phys. Rev. B **34**, 8898 (1986), URL http://link.aps.org/doi/10.1103/PhysRevB.34.8898.

[7] G. D. Mahan and F. Claro, Phys. Rev. B **38**, 1963 (1988), URL http://link.aps.org/doi/10.1103/PhysRevB.38.1963.

[8] G. G. Chen, J. Heat Transfer **118**, 539 (1996), URL http://dx.doi.org/10.1115/1.2822665.

[9] M. E. Siemens, Q. Li, R. Yang, K. A. Nelson, E. H. Anderson, M. M. Murnane, and H. C. Kapteyn, Nature Materials **9**, 26 (2010).

[10] J. A. Johnson, A. A. Maznev, J. Cuffe, J. K. Eliason, A. J. Minnich, T. Kehoe, C. M. S. Torres, G. Chen, and K. A. Nelson, Phys. Rev. Lett. **110**, 025901 (2013), URL http://link.aps.org/doi/10.1103/PhysRevLett.110.025901.

[11] K. T. Regner, A. J. H. McGaughey, and J. A. Malen, Phys. Rev. B **90**, 064302 (2014), URL http://link.aps.org/doi/10.1103/PhysRevB.90.064302.

[12] A. A. Maznev, J. A. Johnson, and K. A. Nelson, Phys. Rev. B **84**, 195206 (2011), URL http://link.aps.org/doi/10.1103/PhysRevB.84.195206.

[13] Y. K. Koh, D. G. Cahill, and B. Sun, Phys. Rev. B **90**, 205412 (2014), URL http://link.aps.org/doi/10.1103/PhysRevB.90.205412.

[14] J. Maassen and M. Lundstrom, Journal of Applied Physics **117**, 135102 (2015), URL http://scitation.aip.org/content/aip/journal/jap/117/13/10.1063/1.4916245.

[15] J. E. Turney, E. S. Landry, A. J. H. McGaughey, and C. H. Amon, Phys. Rev. B **79**, 064301 (2009), URL http://link.aps.org/doi/10.1103/PhysRevB.79.064301.

[16] Recent literature often claims that thermal conduction in inhomogeneous systems disobeys the Fourier law. It would be better to say that it disobeys the local Fourier law $\kappa(\vec{r}-\vec{r}') = \kappa\delta(\vec{r}-\vec{r}')$, or $\tilde{\kappa}(\vec{q}) = \kappa$. The same J. Fourier who realized $\vec{J} = -\kappa\vec{\nabla}T$ also invented the Fourier transforms used here.

[17] P. B. Allen, Phys. Rev. B **90**, 054301 (2014), URL http://link.aps.org/doi/10.1103/PhysRevB.90.054301.

[18] R. E. Peierls, Ann. Phys. **395**, 1055 (1929), URL http://dx.doi.org/10.1002/andp.19293950803.

[19] J. Ziman, *Electrons and Phonons* (Oxford, London, 1960).

[20] E. T. Swartz and R. O. Pohl, Rev. Mod. Phys. **61**, 605 (1989), URL http://link.aps.org/doi/10.1103/RevModPhys.61.605.

[21] D. G. Cahill, P. V. Braun, G. Chen, D. R. Clarke, S. Fan, K. E. Goodson, P. Keblinski, W. P. King, G. D. Mahan, A. Majumdar, et al., Applied Physics Reviews **1**, 011305 (2014), URL http://scitation.aip.org/content/aip/journal/apr2/1/1/10.1063/1.4832615.

[22] Z. Liang and P. Keblinski, Phys. Rev. B **90**, 075411 (2014), URL http://link.aps.org/doi/10.1103/PhysRevB.90.075411.

[23] P. B. Allen and J. L. Feldman, Phys. Rev. B **48**, 12581 (1993), URL http://link.aps.org/doi/10.1103/PhysRevB.48.12581.

[24] F. A. Furtado, C. R. A. Abreu, and F. W. Tavares, AIChE Journal **61**, 2881 (2015), ISSN 1547-5905, URL http://dx.doi.org/10.1002/aic.14803.

[25] F. Müller-Plathe, The Journal of chemical physics **106**, 6082 (1997).

[26] A. Michels, H. Wijker, and H. Wijker, Physica **15**, 627 (1949), ISSN 0031-8914, URL http://www.sciencedirect.com/science/article/pii/0031891449901196.

[27] B. Younglove and H. J. Hanley, Journal of physical and chemical reference data **15**, 1323 (1986).

[28] G. A. Cook, *Argon, Helium, and the Rare Gases* (Intersciences, New York, 1961).

[29] H. J. Hanley, R. D. McCarty, and W. M. Haynes, Journal of Physical and Chemical Reference Data **3**, 979 (1974).

[30] H. Ziebland and J. T. A. Burton, British Journal of Applied Physics **9**, 52 (1958), URL http://stacks.iop.org/0508-3443/9/i=2/a=302.

[31] J.-P. Hansen and L. Verlet, Phys. Rev. **184**, 151 (1969), URL http://link.aps.org/doi/10.1103/PhysRev.184.151.

[32] M. E. Tuckerman, B. J. Berne, and G. J. Martyna, The Journal of chemical physics **94**, 6811 (1991).

[33] D. P. Sellan, E. S. Landry, J. E. Turney, A. J. H. McGaughey, and C. H. Amon, Phys. Rev. B **81**, 214305 (2010), URL http://link.aps.org/doi/10.1103/PhysRevB.81.214305.

[34] M. Omini and A. Sparavigna, Physica B: Condensed Matter **212**, 101 (1995), ISSN 0921-4526, URL http://www.sciencedirect.com/science/article/pii/0921452695000163.

[35] D. A. Broido, M. Malorny, G. Birner, N. Mingo, and D. A. Stewart, Applied Physics Letters **91**, 231922 (2007), URL http://scitation.aip.org/content/aip/journal/apl/91/23/10.1063/1.2822891.

[36] W. Li, J. Carrete, N. A. Katcho, and N. Mingo, Computer Physics Communications **185**, 1747 (2014), ISSN 0010-4655, URL http://www.sciencedirect.com/science/article/pii/S0010465514000484.

[37] G. Fugallo, M. Lazzeri, L. Paulatto, and F. Mauri, Phys. Rev. B **88**, 045430 (2013), URL http://link.aps.org/doi/10.1103/PhysRevB.88.045430.

[38] L. Lindsay, D. A. Broido, and N. Mingo, Phys. Rev. B **82**, 115427 (2010), URL http://link.aps.org/doi/10.1103/PhysRevB.82.115427.

[39] G. Fugallo, A. Cepellotti, L. Paulatto, M. Lazzeri, N. Marzari, and F. Mauri, Nano Letters **14**, 6109 (2014), pMID: 25343716, URL http://dx.doi.org/10.1021/nl502059f.

[40] A. Ladd and L. Woodcock, Molecular Physics **36**, 611 (1978), URL http://dx.doi.org/10.1080/00268977800101791.

[41] F. Clayton and D. N. Batchelder, Journal of Physics C: Solid State Physics **6**, 1213 (1973), URL http://stacks.iop.org/0022-3719/6/i=7/a=012.

[42] D. K. Christen and G. L. Pollack, Phys. Rev. B **12**, 3380 (1975), URL http://link.aps.org/doi/10.1103/PhysRevB.12.3380.

[43] H. Kaburaki, J. Li, S. Yip, and H. Kimizuka, Journal of Applied Physics **102**, 043514 (2007), URL http://scitation.aip.org/content/aip/journal/jap/102/4/10.1063/1.2772547.

[44] A. Chernatynskiy and S. R. Phillpot, Phys. Rev. B **82**, 134301 (2010), URL http://link.aps.org/doi/10.1103/PhysRevB.82.134301.

[45] P. B. Allen, Phys. Rev. B **88**, 144302 (2013), URL http://link.aps.org/doi/10.1103/PhysRevB.88.144302.

[46] B.-Y. Cao and Y.-W. Li, The Journal of Chemical Physics **133**, 024106 (2010), URL http://scitation.aip.org/content/aip/journal/jcp/133/2/10.1063/1.3463699.